

## VIII. PHYSICAL ELECTRONICS AND SURFACE PHYSICS\*

### Academic and Research Staff

Prof. R. E. Stickney  
Dr. T. J. Lee  
Dr. D. L. Fehrs

### Graduate Students

J. C. Batty  
H. C. Juvkam-Wold

D. S. Shupe  
T. Viswanathan

F. J. Walker, Jr.  
S. Yamamoto

### A. MOLECULAR BEAM APPARATUS FOR INVESTIGATIONS OF GAS-SOLID INTERACTIONS

#### 1. Introduction

The nature of the interactions of gases with solid surfaces strongly influences a variety of processes, including electron and ion emission, energy and momentum transfer, oxidation and corrosion, and catalysis. One of the principal experimental techniques for studying gas-solid interactions is the molecular beam,<sup>1-4</sup> and in this report we shall describe an apparatus that has been developed specifically for this purpose. As an illustration of the performance of the apparatus, preliminary results for the scattering of argon atoms from a silicon crystal are included.

#### 2. Apparatus

The principal features of the molecular beam apparatus are the following.

1. The beam is modulated by a mechanical chopper so that a signal of definite frequency and phase is produced, thereby enabling us to utilize a signal-processing technique (e. g. , lock-in detection) that separates the signal from the noise.<sup>5</sup>

2. An aerodynamic nozzle is used to generate the molecular beam because this results in a beam that is both intenser and closer to being monoenergetic than a conventional beam produced by a Knudsen cell.<sup>6</sup>

3. The target mount accommodates single-crystal specimens, and enables us to heat the crystal to high temperature, either in vacuum or in a pure gas, as is necessary to obtain a clean surface.

4. Ultrahigh vacuum components and procedure are employed so that the partial pressures of residual gases in the test chamber are sufficiently low that the surface of

---

\* This work was supported by the National Aeronautics and Space Administration (Grant NGR-22-009-091), the M. I. T. Cabot Solar Energy Fund, and the Joint Services Electronics Programs (U. S. Army, U. S. Navy, and U. S. Air Force) under Contract DA 28-043-AMC-02536(E).

(VIII. PHYSICAL ELECTRONICS AND SURFACE PHYSICS)

the target (i. e., the test specimen) will not become contaminated within the time required to perform a given experimental run.

5. A cesium ion gun is provided so that a controlled amount of cesium may be deposited upon the target surface<sup>7</sup>; this permits us to study the effect of cesium coverage on various gas-solid interactions. An electron gun is used to measure the change in the work function of the target surface resulting from adsorption.<sup>7</sup>

The main components of the apparatus are shown schematically in Fig. VIII-1. The target chamber is a stainless-steel cylinder, 46 cm in diameter, which may be baked because metal gaskets are used in all flanges. [Ultrahigh vacuum systems are generally baked (heated) during evacuation because the elevated temperature accelerates the rate of desorption of gases from the walls and components.] This chamber is evacuated by a diffusion pump (NRC HK4-750, Type 171, with DC-705 silicone oil) that is equipped with a liquid-nitrogen cooled trap (Granville-Phillips 250). A titanium getter surrounded by a second liquid-nitrogen cooled trap is installed within the target chamber to provide additional pumping. A pressure of  $\sim 5 \times 10^{-10}$  Torr is attained when the molecular beam is off, and this value is satisfactory to insure that the target surface will remain essentially clean during an experimental run.<sup>8</sup>

The molecular beam nozzle is a small ( $\sim 0.0254$  mm diameter) aperture formed at the end of a quartz tube (3 mm diameter) by the method devised by Moran.<sup>9</sup> As shown in Fig. VIII-1, a bellows and window are provided so that the position of the nozzle may be varied for alignment purposes. Test gases (Matheson Company, research grade) contained in high-pressure cylinders are supplied to the nozzle through a pressure regulator

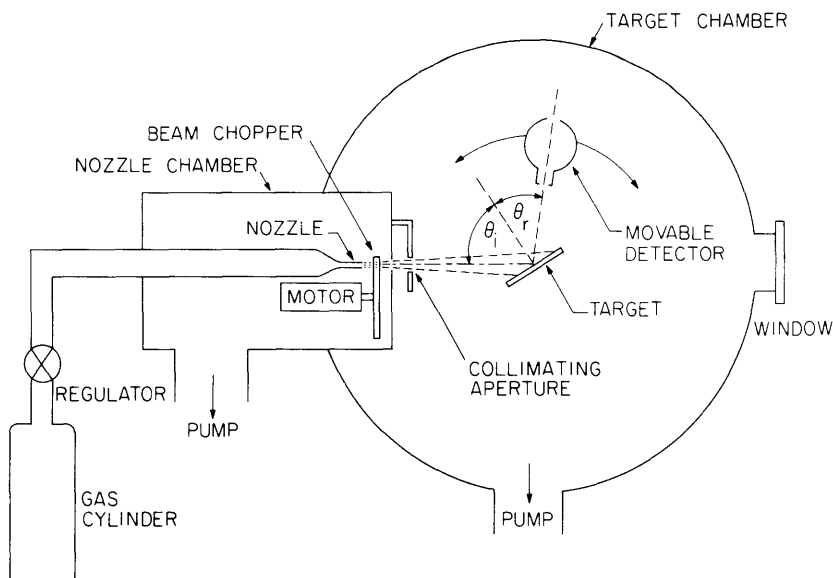


Fig. VIII-1. Schematic diagram of a modulated molecular beam apparatus for investigations of gas-solid interactions.

(VIII. PHYSICAL ELECTRONICS AND SURFACE PHYSICS)

and manifold that may be flushed and evacuated to remove contaminants. The beam is modulated by a slotted disc (the "chopper" in Fig. VIII-1) driven by a small electric motor equipped with bearings that are suitable for vacuum environments (Globe #18A556 hysteresis motor with Barden Bartemp bearings). The modulation frequency and phase are determined from the output signal of a transducer (Electro Products Laboratories, Inc., #3055-A) located at the rim of the chopper. The temperature of the motor is maintained at a safe level (below 50°C) by cooling the motor casing with water flowing in copper tubing.

The nozzle chamber is equipped with a diffusion pump and trap that are the same models as those on the target chamber. The aperture in the partition separating the two chambers is small (~1.6 mm diameter) so that most of the beam gas will be handled by the nozzle-chamber pumps, thereby resulting in a lower pressure in the target chamber. Under normal operating conditions with argon at a nozzle pressure of ~2.36 atm (~20 psig), the pressures in the target and nozzle chambers are  $5 \times 10^{-8}$  Torr and  $5 \times 10^{-4}$  Torr, respectively.

The diameter of the molecular beam at the target is determined by the collimating aperture that is mounted within the target chamber. In the present experiments this aperture has a diameter of 1.6 mm and is located 4.17 cm from the nozzle. Other significant dimensions are nozzle-to-chopper = 1.3 cm, nozzle-to-partition = 1.9 cm, nozzle-to-target = 8.3 cm, and target-to-detector = 7.65 cm.

The target is mounted on a manipulator (Varian model 954-5031) that enables us to vary the position of the target in all three dimensions while maintaining ultrahigh vacuum conditions. With this freedom we may align the target with the beam at any value of  $\theta_1$ , the angle of incidence (Fig. VIII-1), or we may lift the target out of the beam so that we may measure the properties of the direct beam with the detector located on the beam center line behind the normal position of the target.

In the present experiments the target is a single crystal of silicon, the surface being the (111) face. This target has dimensions 10 mm  $\times$  5 mm  $\times$  1 mm, and is held at each end by tantalum straps to allow AC current to be passed directly through the crystal so that temperatures up to the melting point (1688°K) may be attained. The results of low-energy electron diffraction studies of (111) Si show that a clean surface may be obtained simply by heating it in ultrahigh vacuum.<sup>10</sup> The crystal is electro-polished before installation according to the procedure recommended by Turner.<sup>11</sup>

An ion gun is used to deposit known amounts of cesium upon the target, and an electron gun enables us to measure the change in the target work function resulting from adsorption. (Since design and operation of these guns have been described in a recent publication,<sup>7</sup> we shall not repeat the details here.) Both guns are so located that they are focussed on the target when it is lifted out of the beam. After deposition of the desired amount of Cs, the target may be lowered quickly into the beam so that we can

(VIII. PHYSICAL ELECTRONICS AND SURFACE PHYSICS)

measure the effect of Cs coverage on the scattering of rare gases from (111) Si. We expect that the presence of Cs on the target surface will cause a significant change in the scattering patterns because (a) the mass of Cs is more than four times greater than that of Si, and (b) the Cs adatoms will strongly perturb both the magnitude and the shape (e.g., the contour or microscopic roughness) of the intermolecular potential experienced by the rare gas atoms when colliding with the target. A special advantage of the choice of Cs and (111) Si is that this system has been studied in considerable detail both by low-energy electron diffraction<sup>10</sup> and by contact-potential methods.<sup>12, 13</sup>

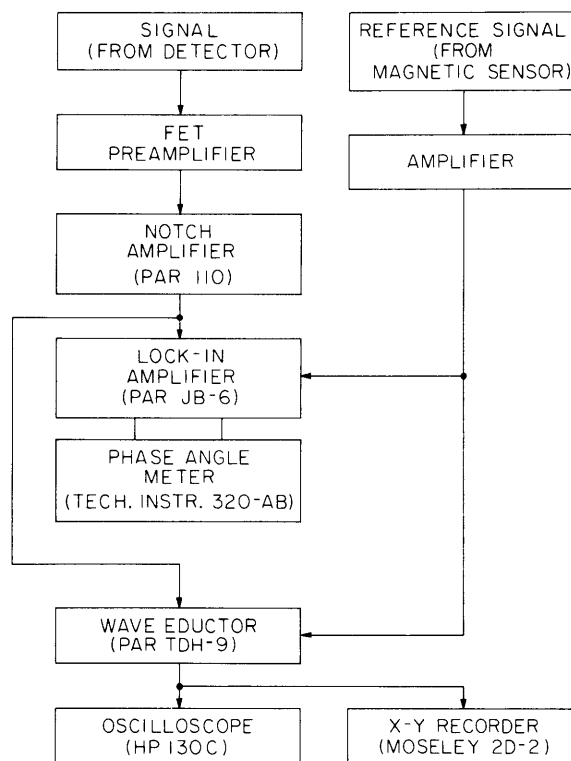


Fig. VIII-2. Block diagram of detector electronics.

The detector and its circuitry (Fig. VIII-2) are essentially identical to those employed by Hinchey and Malloy,<sup>14</sup> and we have described them in detail elsewhere.<sup>4,5</sup> The detector is a Bayard-Alpert ionization gauge (General Electric Model 22GT102) so mounted that it may be rotated about the target to measure the scattering pattern. The acceptance angle of the detector is determined by the size of the aperture at the entrance to the detector, and, at present, the diameter of this aperture is 0.7 mm. By providing a larger aperture at the rear of the detector (Fig. VIII-1), we insure that the majority of the atoms passing through the entrance may traverse the detector without collisions

with walls or other molecules, and the detector output signal will be proportional to the density of the scattered gas. The advantage of this type of "through-flow detector" is that measurements of the phase angle of the signal provide information on the mean speed of the scattered atoms.<sup>4, 5, 14</sup>

A block diagram of the electronic components of the detection system is shown in Fig. VIII-2. The detector signal first goes to a FET preamplifier having an input impedance of 100 M $\Omega$  and a gain of  $\sim 10$ . Next, there is a notch amplifier that rejects 120-Hz noise and has a gain of  $10^2$ - $10^4$  for the signal. From this point the signal may be fed either to a lock-in amplifier or to a wave eductor. Since the lock-in amplifier has been used in the preliminary experiments, we shall concentrate on it in the present discussion. The principal feature of this unit is that it separates signal from noise by mixing the detector signal with the reference signal and then averaging the result from 0.1 to 3 seconds. The amplitude of the output signal is proportional to the density of the scattered atoms, and the phase angle is a measure of the mean speed of these atoms. (A detailed discussion of the phase angle and its interpretation is omitted because we have treated this subject elsewhere.<sup>5</sup>)

The wave eductor is a multichannel signal-averaging device that is capable of recording the waveform of a signal that originally is obscured by noise. Although the information obtained with this unit is more detailed than that obtained with the lock-in amplifier, it is difficult to realize this advantage when the signal-to-noise ratio is extremely low. Our present plan is to use the lock-in amplifier to measure the scattered beam and reserve the wave eductor for measurements of the velocity distribution of the direct beam.

### 3. Direct Beam Data

The data presented in Figs. VIII-3 and VIII-4 were obtained by lifting the target so that the beam may impinge directly upon the detector when it is rotated into the beam path. The lock-in amplifier was used in the present tests, and the beam gas was argon.

The profile of the beam is shown in Fig. VIII-3 for two values of  $p_0$ , the pressure upstream of the nozzle. The ordinate is the amplitude of the output signal of the lock-in amplifier, and it is proportional to the density of the beam at the position of the detector. Since the abscissa is the angular position of the detector for rotation about the center line of the target chamber, it is not exactly equal to the divergence of the beam. Taking this into account, we have included in Fig. VIII-3 the positions of the umbra and penumbra as calculated from the dimensions of the beam path and collimating apertures. Notice that the measured profile agrees qualitatively with the calculations.

With the detector positioned on the center line of the beam, the data of Fig. VIII-4 were obtained by varying the speed of the chopper motor for three

(VIII. PHYSICAL ELECTRONICS AND SURFACE PHYSICS)

values of nozzle pressure. Since there are 4 equally spaced slots in the chopper disc and 6 poles in the motor, the modulation frequency is 4/3 the motor driving frequency. The decrease in signal with increasing frequency is in agreement with the general trend of the computational results of Harrison, Hummer, and Fite.<sup>15</sup>

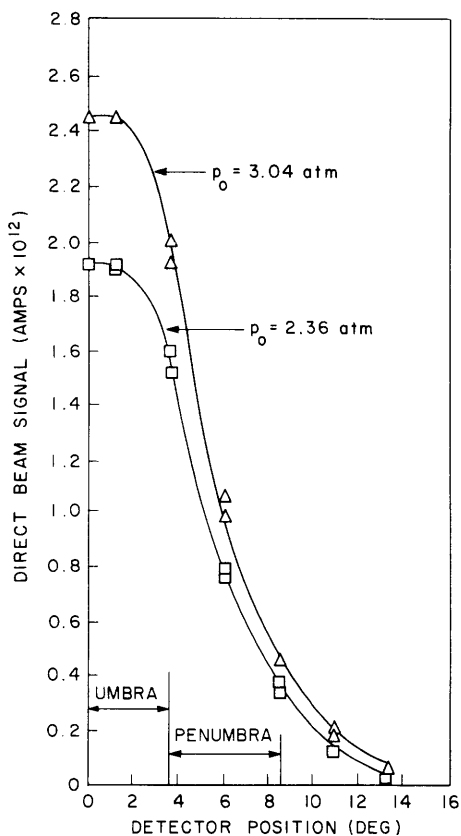


Fig. VIII-3.

Measurements of the profile of an argon beam for two values of  $p_0$ , the nozzle source pressure. Modulation frequency,  $f$ , is 172 Hz.

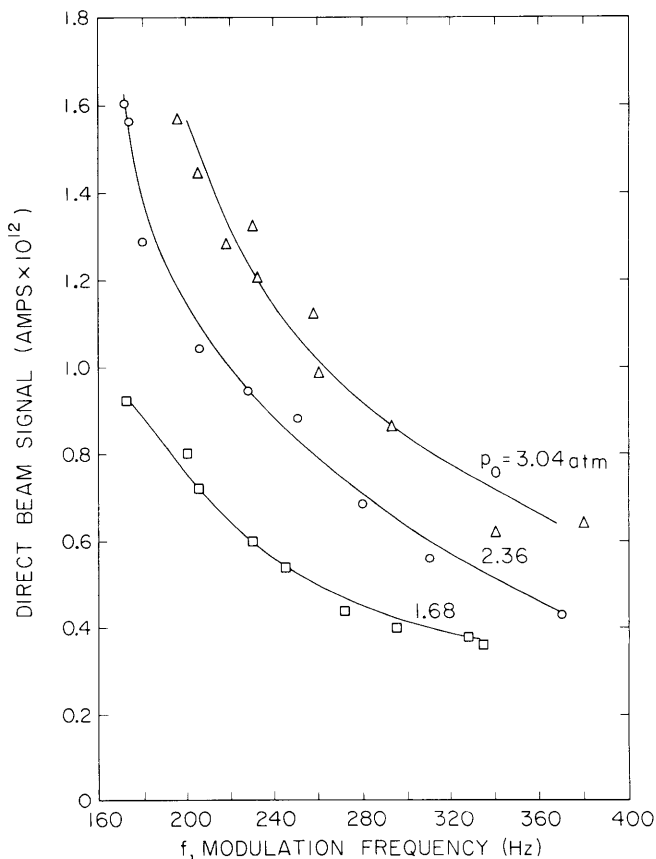


Fig. VIII-4.

Measurements of the dependence of the intensity of a direct argon beam on modulation frequency for 3 values of  $p_0$ , the nozzle source pressure.

4. Scattering Data

The performance of the apparatus was checked by scattering a beam of argon atoms from a surface that was known to be heavily contaminated with adsorbed residual gases. Under these conditions we would expect the scattering pattern to be diffuse (i. e., to be proportional to  $\cos \theta_r$ ), and, as shown in Fig. VIII-5, the measured pattern appears to be diffuse except at large values of  $\theta_r$ . A possible

(VIII. PHYSICAL ELECTRONICS AND SURFACE PHYSICS)

explanation for the deviation from the diffuse pattern is that the signal-to-noise ratio decreases with increasing  $\theta_r$  to the extent that the accuracy of the measurements is poor. Attempts are now being made to correct this problem.

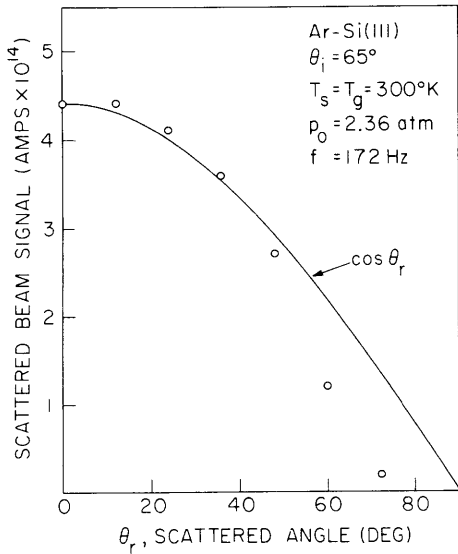


Fig. VIII-5. Experimental pattern for the scattering of an argon beam from a contaminated (111) silicon crystal. The surface of the crystal was allowed to be contaminated by residual gases so that we could determine whether a diffuse pattern (solid curve labeled  $\cos \theta_r$ ) would be observed.

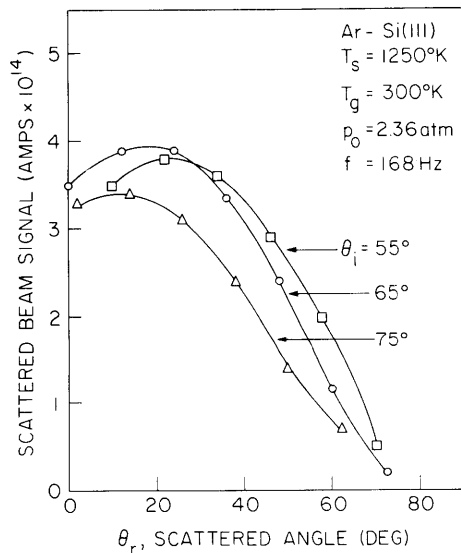


Fig. VIII-6. Experimental patterns for the scattering of an argon beam from a "clean" (111) silicon crystal for 3 values of  $\theta_i$ , the angle of incidence.

The scattering patterns shown in Fig. VIII-6 for three angles of incidence were obtained after the target was held at  $1250^\circ\text{K}$  for 10 hours in an attempt to obtain a clean surface. In these cases the patterns are no longer diffuse, and their general appearance is similar to that observed by other investigators<sup>3, 14</sup> for various gases and target materials. Notice that the maxima of the patterns shift toward lower values of  $\theta_r$  as  $\theta_i$  increases. It is possible that this trend may be associated with an increase in the

(VIII. PHYSICAL ELECTRONICS AND SURFACE PHYSICS)

normal component of momentum of the argon atoms, as suggested by the "hard-cube" model proposed by Logan, Keck, and Stickney,<sup>16</sup> but quantitative comparisons cannot be made because the mass ratio of argon/silicon is too large for the "hard-cube" model to be valid in its present form.

S. Yamamoto, R. E. Stickney

References

1. N. F. Ramsey, Molecular Beams (Oxford University Press, London and New York, 1956).
2. W. L. Fite and S. Datz, in Annual Reviews of Physical Chemistry, Vol. 14 (Annual Reviews, Inc., Palo Alto, Calif., 1963), pp. 61-88.
3. J. N. Smith and H. Saltsburg, in Fundamentals of Gas-Surface Interactions, edited by H. Saltsburg et al. (Academic Press, Inc., New York, 1967), pp. 370-391.
4. R. E. Stickney, in Advances in Atomic and Molecular Physics, Vol. III, edited by D. R. Bates and I. Estermann (Academic Press, Inc., New York, 1968), pp. 143-204.
5. S. Yamamoto and R. E. Stickney, J. Chem. Phys. **47**, 1091 (1967).
6. For a discussion of nozzle beams, see J. B. Anderson, R. P. Andres, and J. B. Fenn, in Advances in Atomic and Molecular Physics, Vol. I, edited by D. R. Bates and I. Estermann (Academic Press, Inc., New York, 1965), pp. 345-389; and E. L. Knuth, Appl. Mech. Rev. **17**, 751 (1964).
7. D. L. Fehrs and R. E. Stickney, Surface Sci. **8**, 267 (1967).
8. For a detailed discussion of the maintenance of clean surfaces in ultra-high vacuum systems, see R. W. Roberts and T. A. Vanderslice, Ultrahigh Vacuum (Prentice-Hall, Inc., Englewood Cliffs, N. J., 1963), Chap. 5.
9. J. P. Moran, Ph.D. Thesis, Massachusetts Institute of Technology, September 1967.
10. J. J. Lander and J. Morrison, in Progress in Solid State Chemistry, Vol. II (Pergamon Press, New York, 1965), pp. 26-116.
11. D. R. Turner, J. Electrochem. Soc. **105**, 402 (1958).
12. F. G. Allen and G. W. Gobeli, in Proc. International Conference on the Physics of Semiconductors (Adlard and Son, Ltd., 1962), pp. 818-826.
13. R. F. Weber, in Report on Twenty-seventh Annual Conference on Physical Electronics, Massachusetts Institute of Technology, Cambridge, Mass., March 21-23, 1967, pp. 38-46.
14. J. J. Hinchey and E. S. Malloy, in Fundamentals of Gas-Surface Interactions, H. Saltsburg et al. (eds.), op. cit., pp. 448-460.
15. H. Harrison, D. G. Hummer, and W. L. Fite, J. Chem. Phys. **41**, 2567 (1964).
16. R. M. Logan and R. E. Stickney, J. Chem. Phys. **44**, 195 (1966); R. M. Logan, J. C. Keck, and R. E. Stickney, in Proc. 5th International Symposium on Rarefied Gas Dynamics, Vol. I (Academic Press, Inc., New York, 1967), pp. 49-66; R. E. Stickney, R. M. Logan, S. Yamamoto, and J. C. Keck, in Fundamentals of Gas-Surface Interactions, H. Saltsburg et al. (eds), op. cit., pp. 422-434.



B. EQUILIBRIUM MODEL OF THE REACTION OF A GAS WITH A  
SOLID TO FORM VOLATILE PRODUCTS: STEADY-STATE  
OXIDATION OF TUNGSTEN

1. Introduction

This study represents an initial step in a research program on the kinetics of chemical reactions occurring at the gas-solid interface. The scope of the program is reduced and simplified by the fact that we shall concentrate on reactions in which the products are sufficiently volatile that a new solid phase does not form at the surface, as is the case at high temperatures and low pressures for certain gas-solid systems.<sup>1</sup> One of the first questions that should be answered for any steady-state reaction of this kind is, Does the measured composition of the volatile products agree with the composition calculated on the basis of equilibrium considerations? A unique answer is not possible, however, because the application of equilibrium thermodynamics to nonequilibrium processes generally requires additional assumptions. Some of these assumptions are considered here in the development of an "equilibrium model." As an illustration of the application of the model, numerical results are presented for the reaction of oxygen with tungsten.

There are several reasons for selecting the oxygen-tungsten reaction as the first application of the equilibrium model. (i) Mass spectrometric data on the volatile products of gas-solid reactions exist in greater quantity for oxygen-tungsten than for any other gas-metal system.<sup>1-5</sup> (ii) The thermodynamic property data that are necessary to compute equilibrium constants for gaseous oxides are available for oxygen-tungsten, whereas these data are not available for all gas-metal systems. (iii) Recently, thermionic emission measurements of the adsorption and desorption of oxygen on tungsten have been performed in our laboratory.<sup>6,7</sup> (iv) The oxidation of tungsten at high temperatures and low pressures is encountered in various technological areas, including thermionic energy conversion,<sup>8</sup> ion propulsion,<sup>9</sup> and high-temperature gas dynamics.<sup>10</sup>

2. Description of the Equilibrium Model

The dotted line in Fig. VIII-7 represents the boundary of the control volume that will be utilized. We shall assume that (i) the y and z dimensions of the control volume are unity so that a unit area of solid surface is enclosed, (ii) the x dimension is sufficiently small that the fluxes of matter across the horizontal faces of the control volume are negligible relative to the fluxes across the vertical faces, (iii) the center line of the control volume remains fixed to the solid surface, even when the surface recedes into the solid because of the loss of material by evaporation. As a result of the last assumption, the control volume will achieve steady-state conditions when the solid is consumed at a uniform rate and the states of the solid and gas at  $-\infty$  and  $+\infty$ , respectively, are

(VIII. PHYSICAL ELECTRONICS AND SURFACE PHYSICS)

maintained constant.

In order to reduce the number of terms in the following equations, we shall assume that the solid is a pure element, M, whereas the gas is a perfect-gas

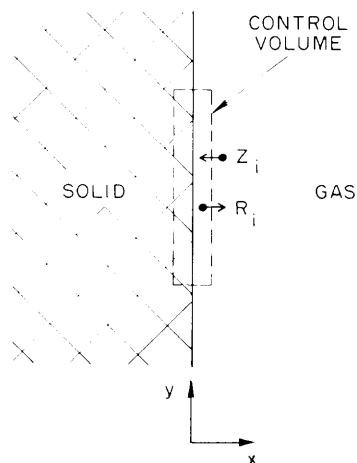


Fig. VIII-7. Schematic representation of a gas-solid interface.

mixture consisting only of atoms, A, and diatomic molecules, A<sub>2</sub>. The possible chemical reactions may be represented by a general expression



where the permissible values of x and y depend on the chemical nature of the specific choice of gas and solid. The corresponding expression for the equilibrium constants is

$$K_{M_x A_y} = p_{M_x A_y} / (p_{A_2})^{y/2}, \quad (2)$$

where  $p_{M_x A_y}$  and  $p_{A_2}$  are the equilibrium partial pressures of gaseous species  $M_x A_y$  and  $A_2$ , respectively. If the free energies of formation,  $\Delta F_{M_x A_y}$ , are known for the reactions described by Eq. 1, then the equilibrium constants may be evaluated from

$$\ln K_{M_x A_y} = -\Delta F_{M_x A_y} / RT, \quad (3)$$

where R and T are the gas constant and temperature, respectively.

If the state of the gas just outside the right-hand boundary of the control volume is known, we may compute  $Z_{M_x A_y}$ , the flux of each species into the control volume, by means of kinetic theory. From these fluxes we may determine the total flux of A into the control volume,

$$(Z_A)_{\text{total}} = \sum_{x,y} y Z_{M_x A_y} \quad (4)$$

Similarly, the total flux of A leaving the control volume at the right-hand boundary is

$$(R_A)_{\text{total}} = \sum_{x,y} y R_{M_x A_y}, \quad (5)$$

where  $R_{M_x A_y}$  represents the unknown flux of each species corresponding to the state of the gas located just inside the boundary. If steady-state conditions exist and if the amount of A crossing the other boundaries is negligible, then

$$(R_A)_{\text{total}} = (Z_A)_{\text{total}} \quad (6)$$

[Note that there will be a flux of species A across the left-hand boundary if the gas absorbs in the solid, but the magnitude of this flux would be negligible in most cases.] If there are  $n$  possible chemical species, then Eq. 6 gives us one equation involving  $n$  unknowns. By assuming that chemical equilibrium exists inside the control volume, Eq. 2 provides the remaining  $n-1$  equations that are necessary to determine the state of the gas just inside the right-hand boundary. Since kinetic theory provides the equations that relate fluxes to partial pressures, we have a sufficient number of equations to solve the problem.

The procedure outlined above is especially simple in the limiting case of free molecule flow (that is, the case for which the gas density is sufficiently low that the mean-free path is much larger than the characteristic dimension of the solid). In this case the state of the gas just outside the boundary of the control volume is the same as the state at  $+\infty$ , since there are no gas-phase collisions in the vicinity of the solid to create a gradient or to scatter the evaporating species back toward the surface. Therefore, if the gas at  $+\infty$  is in an equilibrium state, the flux of species  $i$  into the control volume is given by the Hertz-Knudsen equation,

$$Z_i = \frac{p_i}{\sqrt{2\pi m_i kT}} = 3.51 \times 10^{22} \frac{p_i}{\sqrt{M_i T}} \text{ cm}^{-2} \text{ sec}^{-1}, \quad (7)$$

where  $p_i$ ,  $m_i$ , and  $M_i$  are, respectively, the partial pressure (Torr), mass (grams), and molecular weight of species  $i$ , and  $T$  is the temperature ( $^{\circ}\text{K}$ ). [Note: Eq. 7 is valid only if the rate of recession of the solid surface is sufficiently low to cause the velocity of the control volume to be negligible in comparison with the mean speed of the gas molecules, as is generally the case for practical applications.] Since we

## (VIII. PHYSICAL ELECTRONICS AND SURFACE PHYSICS)

assume that equilibrium between the gas and solid exists within the control volume, Eq. 7 may also be applied to the fluxes leaving the control volume if the appropriate values of  $T$  and  $p_i$  are used. [Note: the temperatures of the gas ( $T_g$ ) and the solid ( $T_s$ ) are not necessarily equal.] In this case Eq. 6 may be written

$$\sum_i y_i \left( \frac{s_i p_i}{\sqrt{M_i T_s}} \right)_{\text{out}} = \sum_i y_i \left( \frac{s_i p_i}{\sqrt{M_i T_g}} \right)_{\text{in}}, \quad (8)$$

where  $s_i$ , the "sticking probability," has been introduced to account for the fact that only a fraction of the particles that collide with a solid surface will come to equilibrium with the solid before evaporating.<sup>11</sup> The sticking coefficient also appears in the evaporation rates because the principle of detailed balancing leads to the conclusion that the evaporation probability must equal the sticking probability under equilibrium conditions. Since there are very little reliable data on the magnitude of  $s_i$  for various gas-solid systems, we are forced to assume in the following calculations that  $s_i$  is unity for all species. (For a review of the existing experimental data on  $s_i$ , see Hayward and Trapnell.<sup>11</sup>)

### 3. Results for the Reaction of Oxygen with Tungsten

Schissel and Trulson<sup>2</sup> recently have used a mass spectrometer to measure the volatile products of the oxygen-tungsten reaction for steady-state conditions in the temperature range 1400-3150°K. Since the oxygen pressure was sufficiently low ( $p_{O_2} \leq 2.1 \times 10^{-4}$  Torr) that free-molecular flow conditions were assured, the temperature of the gas impinging upon the tungsten surface was equal to the temperature of the water-cooled chamber walls (~290°K), and the impinging flux of O is negligible in comparison with that for  $O_2$ . The ionization section of the mass spectrometer was located so that a fraction of the reaction products evaporating from the tungsten surface could pass directly through it without undergoing collisions with walls, electrodes, or other molecules. An example of Schissel and Trulson's data is given in Fig. VIII-8, and we see that the principal products are O, WO,  $WO_2$ ,  $WO_3$ ,  $W_2O_6$ , and  $W_3O_9$ . (Note: they were unable to obtain data on  $O_2$  because the background gas was predominately  $O_2$ .)

Also shown in Fig. VIII-8 are the predictions of the equilibrium model for corresponding conditions. The 10 species that were accounted for in the computations are listed in Table VIII-1, together with their enthalpies and entropies of formation. The enthalpy and entropy of each species are the values for the temperature at which the evaporation rate of the particular species is largest according to the experimental data shown in Fig. VIII-8. Since the uncertainty of the existing values of  $\Delta H$  and  $\Delta S$  exceed the variation of these properties with temperature in the range of interest (1400-3150°K), we have applied the values given in Table VIII-1 without correction to compute the

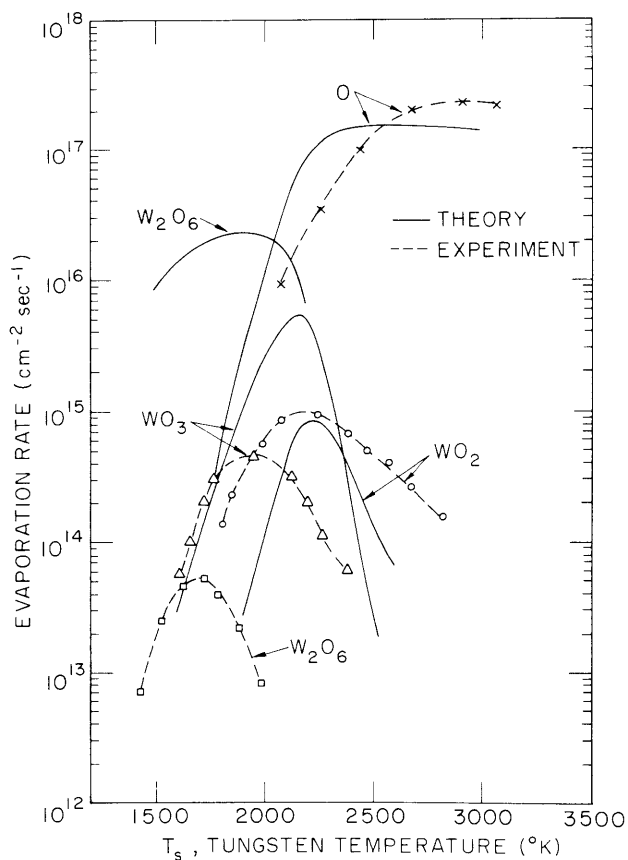


Fig. VIII-8.

Evaporation rates of volatile products formed in the reaction of oxygen with tungsten. The experimental data are those of Schissel and Trulson,<sup>2</sup> whereas the theoretical results are based on the "equilibrium model." In both cases, the temperature and pressure of the oxygen gas are, respectively, 290°K and  $2.1 \times 10^{-4}$  Torr; therefore, the incident flux,  $Z_{O_2}$ , is  $7.7 \times 10^{16}$  molecules  $\text{cm}^{-2} \text{sec}^{-1}$ .

Table VIII-1. Enthalpies and entropies of formation for oxygen and various tungsten oxides.

Species	$\Delta H$ (kcal/gmole)	$\Delta S$ (cal/gmole-deg)	Reference
O	61.3	16.0	14
WO	99.0	25.0	14
WO <sub>2</sub>	17.6	6.0	14
WO <sub>3</sub>	-70.0	-13.5	14
W <sub>2</sub> O <sub>6</sub>	-272.5	-55.0	15
W <sub>3</sub> O <sub>8</sub>	-400.9	-90.5	15
W <sub>3</sub> O <sub>9</sub>	-458.0	-100.0	14
W <sub>9</sub> O <sub>12</sub>	-635.0	-145.0	14

Note: The data for each species correspond to the temperature at which the rate of formation of that species is greatest according to the experimental data shown in Fig. VIII-10.

(VIII. PHYSICAL ELECTRONICS AND SURFACE PHYSICS)

equilibrium constants through Eq. 3 with  $\Delta F_{W_x O_y} = \Delta H_{W_x O_y} - T_s \Delta S_{W_x O_y}$ . This provides 9 equations in terms of the 10 unknown partial pressures; the tenth equation follows from Eq. 8 with the assumption that  $s_i$  is unity for all species. A digital computer was used to obtain numerical solutions of this set of equations.

The principal features of the comparison of results in Fig. VIII-8 are the following.

1. For each of the observed species the theoretical curves lie above the corresponding experimental curves, just as one would expect if equilibrium were not completely attained. (Although inaccuracies in the thermodynamic data given in Table VIII-1 could contribute to this discrepancy, the effect is too large to be due to this factor alone.)
2. The agreement between theory and experiment is surprisingly close with respect to the temperatures at which each species attains its maximum evaporation rate.
3. Although the curves for O are similar in form, the experimental curve is shifted to higher temperatures by an amount that we believe is too large to attribute to inaccuracies in either the experimental data or the theoretical calculations.

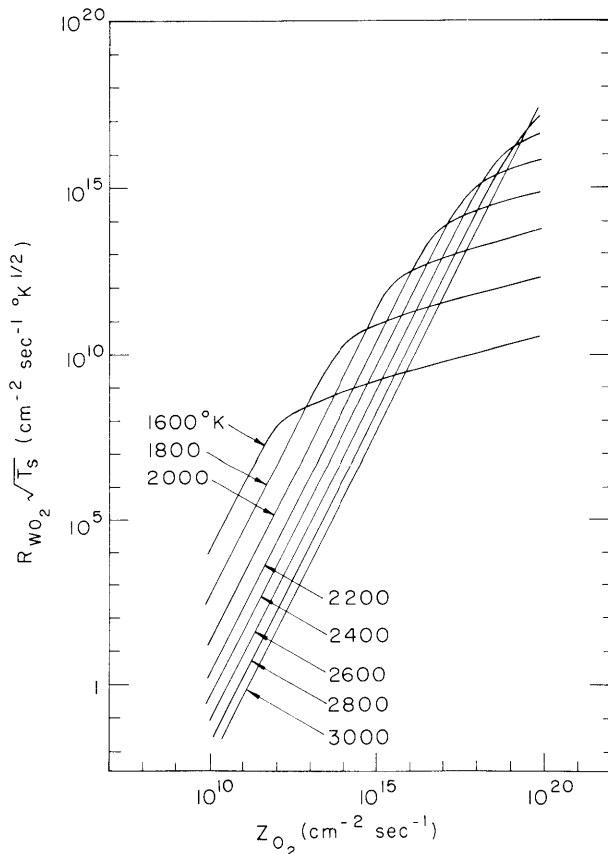


Fig. VIII-9. Dependence of the evaporation rate of  $WO_2$  on the incident  $O_2$  flux for tungsten temperatures in the range 1600-3000°K. (Based on the "equilibrium model.")

to higher temperatures by an amount that we believe is too large to attribute to inaccuracies in either the experimental data or the theoretical calculations.

4. Although the experimental and theoretical curves for O do not approach the same limiting value at high temperatures, we believe that this discrepancy is insignificant in the present case because a reasonable error in either the pressure measurements or mass-spectrometer sensitivity factor would account for it.

Schissel and Trulson also present data on the dependence of the rates of formations of the different species on  $Z_{O_2}$ , the flux of  $O_2$  upon the tungsten surface. Their data for  $WO_2$  indicate that a first-order dependence exists over a large portion of the temperature range, but, at the highest temperatures, the order increases to at least a second-order dependence. A similar trend is predicted by the equilibrium model; for example, the

(VIII. PHYSICAL ELECTRONICS AND SURFACE PHYSICS)

results given in Fig. VIII-9 show that for a specific value of  $Z_{O_2}$ , the order (that is, the slope) indeed increases for a sufficient increase in temperature. We have observed the same general agreement for O and  $WO_3$ .

A question that has practical significance is, How does the rate of erosion of tungsten by oxygen vary with the temperature of the solid and the flux of oxygen upon the surface?

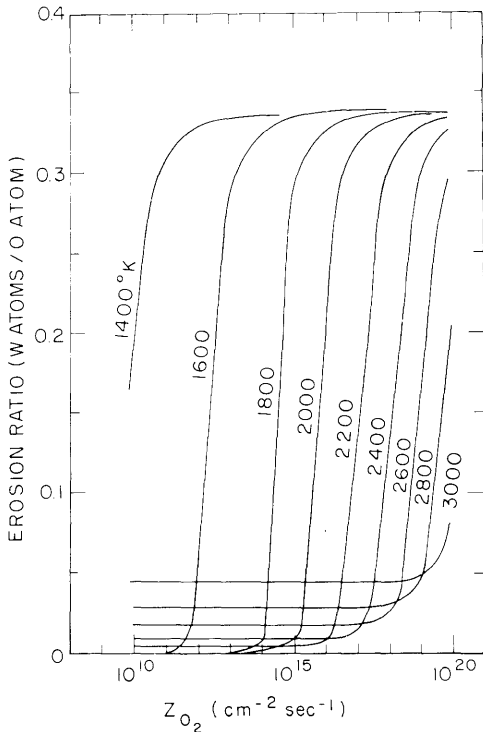


Fig. VIII-10. Dependence of the tungsten-oxygen erosion ratio on incident  $O_2$  flux for tungsten temperatures in the range 1400-3000°K. (Based on the "equilibrium model.") The erosion ratio represents the number of tungsten atoms removed per oxygen atom.

The answer provided by the "equilibrium model" is given in Fig. VIII-10, where the ordinate (erosion ratio) represents the average number of tungsten atoms removed per oxygen atom. For high fluxes (pressures), the erosion ratio is  $\sim 0.33$  because the dominant species is  $WO_3$  and its polymers. For low fluxes, the erosion ratio deviates from zero as the temperature increases, because of the formation of a small amount of  $WO$ .

#### 4. Conclusions

We have described a model that may be used to predict the "equilibrium" rates of formation of volatile products in gas-solid reactions. The model is more general than indicated herein, since it is a generalization of the existing models of surface ionization<sup>12</sup> and catalytic processes.<sup>13</sup>

(VIII. PHYSICAL ELECTRONICS AND SURFACE PHYSICS)

From a comparison of the "equilibrium" predictions and existing experimental data for the reaction of oxygen with tungsten, we conclude that equilibrium is not attained completely even in the most elementary step of the reaction – the dissociation of oxygen. Additional comparisons are being made, and kinetic studies, both theoretical and experimental, are being considered for the future.

J. C. Batty, R. E. Stickney

References

1. P. Kofstad, High Temperature Oxidation of Metals (John Wiley and Sons, Inc., New York, 1966), pp. 247-260.
2. P. O. Schissel and O. C. Trulson, *J. Chem. Phys.* 43, 737 (1965).
3. J. B. Berkowitz-Mattuck, A. Buchler, J. L. Engelke, and S. N. Goldstein, *J. Chem. Phys.* 39, 2722 (1963).
4. Yu. G. Ptushinskii and B. A. Chuikov, *Surface Sci.* 6, 42 (1967); 7, 90 (1967).
5. B. M. McCarroll, *J. Chem. Phys.* 46, 863 (1967). (Note: this paper contains a very complete list of references on the oxygen-tungsten studies performed before 1967.)
6. W. Engelmaier and R. E. Stickney, *Surface Sci.* (to be published).
7. W. Greaves and R. E. Stickney, *Surface Sci.* (to be published).
8. D. Lieb and S. S. Kitrilakis, in Proc. Thermionic Conversion Specialist Conference (1966 IEEE Conference), pp. 348-354; F. Ruffeh, D. Lieb, and F. Fraim, in Proc. Thermionic Conversion Specialist Conference (1967 IEEE Conference), pp. 25-28.
9. A. Y. Cho and H. Shelton, *AIAA J.* 2, 2135 (1964).
10. D. E. Rosner and H. D. Allendorf, *J. Electrochem. Soc.* 114, 305 (1967); G. A. Etemad, *AIAA J.* 4, 1543 (1966); B. W. Marshall, *AIAA J.* 4, 1899 (1966).
11. D. O. Hayward and B. M. W. Trapnell, Chemisorption (Butterworths Scientific Publications, London, 2d edition, 1964), Chap. 3.
12. I. Langmuir, *Phys. Rev.* 43, 224 (1933).
13. G. Ehrlich, *J. Chem. Phys.* 31, 1111 (1959).
14. JANAF Tables of Thermochemical Data, edited by D. R. Stull (Dow Chemical Company, Midland, Michigan, 1965).
15. R. J. Ackerman and E. G. Rauh, *J. Chem. Phys.* 67, 2596 (1963).